An AUV Survey in the Littoral Zone: Small-Scale Subsurface Variability Accompanying Synoptic Observations of Surface Currents

Manhar R. Dhanak, P. Edgar An, and Ken Holappa

***Abstract*—A survey of small-scale subsurface variability within the synoptic observational field of an ocean surface current radar (OSCR) using an autonomous underwater vehicle (AUV) is described. The survey involved observation of a developing upper mixed layer in a littoral zone off southeast Florida, on the edge of a strong Florida current during the summer of 1999. Complimentary *in situ* observations from a bottom-mounted acoustic Doppler current profiler (ADCP), conductivity-temperature (CT) chain arrays, atmospheric measurements from a surface buoy, and CTD and ADCP observations from a surface ship provided the background to the survey. The AUV, the Ocean Explorer, equipped with a CTD, downward and upward looking ADCPs, and a small-scale turbulence package, was used to conduct a continuous 12-h survey of small-to-fine-scale variability within a few grid cells of the surface current radar field. The vehicle repeatedly sampled the same grid in a set pattern at a fixed mid-water depth. Maps of developing spatial distribution of current, salinity, temperature, and rate of dissipation have been developed using the AUV-based observations. The observed features in the current field compare well with the OSCR and the bottom-mounted ADCP measurements. The observations revealed a strong presence of a near-tidal period (10-h) oscillation in the current field accompanying a northward propagating shear wave along the edge of the Florida current and other features, including the presence of patches with relatively high dissipation rates during the survey. The data set acquired provides simultaneous maps of subsurface structure, including rate of dissipation of kinetic energy and synoptic field observations of high-resolution surface current. The application of the AUV in this oceanographic survey represents a step in the direction of developing a multivehicle ocean sampling system.**

***Index Terms*— AUV, CTD, currents fields, oceanographic survey, OSCR, subsurface, turbulence.**

I. Introduction

SYNOPTIC observation of sea-surface temperature or sea color from remote satellites and of surface current using high-frequency (HF) Doppler radars are of significant importance to our understanding of ocean dynamics and to ocean modeling in a coastal environment. Typically, these remote sensors provide measurements over regions extending over tens or hundreds of square kilometers at a specified resolution. For example, existing ocean surface current radars (OSCRs) provide surface current measurements over 700 km^2 approximately with a resolution of 1 km when operating in HF mode and over 40 km^2 with a resolution of 250 m in Very High Frequency (VHF) mode [1].

Central to this question about radar-derived surface currents is their relationship to a subsurface structure. Recent studies have shown good agreement with moored subsurface current meters. For example, Shay *et al.* [2] found rms differences of 7 $cm{\cdot}s^{-1}$ between surface currents and those at 4 m beneath the surface. More recently, moored and shipboard current measurements from a downward-looking acoustic Doppler current profiler (ADCP) at 50 m revealed rms differences of 11–15 $cm{\cdot}s^{-1}$ between VHF-radar surface and 4 m from the 29-day measurements acquired during the July 1999 experiment [3]. One of the interesting aspects of this data set is the marked variability in the surface velocity where the ambient vorticity was quite large [4].

The coastal variability, however, occurs over a broad spectrum of temporal and spatial scales and generally involves subsurface processes. Thus, supplementary observations in the water column and the near-surface layers of the atmosphere are needed to determine, for example, the characteristics of a physical process associated with a synoptic observation. A range of instruments capable of resolving microstructure to mesoscale variations in one or more of these variables may typically be needed [5] and deployed from a variety of measurement platforms.

Here we describe use of an autonomous underwater vehicle (AUV) for sampling small O(10 m) to microstructure scale O(0.01 m) variability in the water column in conjunction with the concurrent synoptic measurement of surface currents in an extended 12-h observation of the upper mixed layer in the littoral zone on the edge of a strong Florida Current during summer 1999 [3]. The subsurface *in situ* measurements include bulk temperature, salinity, velocity profiles, and small-scale turbulence. Spatial maps of these quantities, including *in situ* rate of dissipation are presented together with simultaneous maps of synoptic surface velocity. Acquisition of such simultaneous data sets provides a capability to study turbulent processes and sub grid scale mixing and its relationship to larger scale flow structures. A future near real-time ocean observation system would involve a number of such AUV-based measurement platforms as elements in oceanographic sampling networks [6]. The capability described here demonstrates, in part, the

Manuscript received January 29, 2001; revised September 19, 2001. This work was supported by the Office of Naval Research (Program Manager: Dr Thomas Curtin).

M. Dhanak and P. E. An are with the Department of Ocean Engineering, Florida Atlantic University, Boca Raton, FL 33431 USA.

K. Holappa was with with the Department of Ocean Engineering, Florida Atlantic University, Boca Raton, FL 33431 USA. He is now with Ocean Sensor Systems, Coral Springs, FL 33065 USA.

Publisher Item Identifier S 0364-9059(01)10367-5.

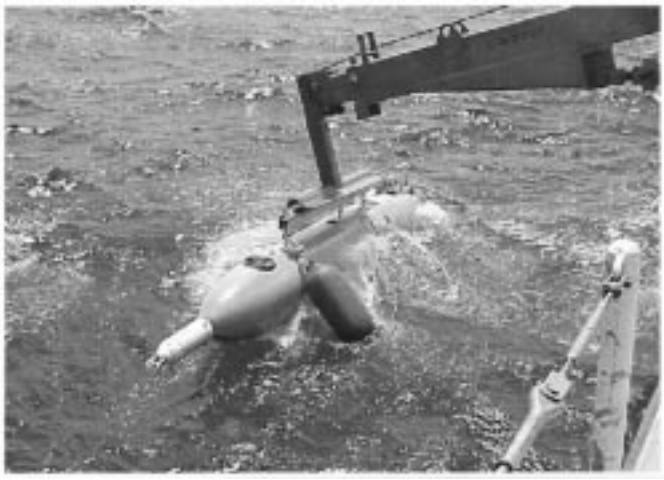

Fig. 1. The OEX AUV. The turbulence package and the upward-looking ADCP are visible in the picture.

potential of an element of such a network. The total network would potentially provide a much larger spatial coverage and/or at a faster rate and represent a powerful subsurface capability that would compliment synoptic remotely sensed observations in support of real-time oceanography. A number of other independent efforts toward the application of AUVs as reliable mobile platforms for oceanographic instruments have been undertaken in the U.S. and Europe [7]–[16].

In the work of An *et al.* [10] and Dhanak and Holappa [9], development efforts in application of Florida Atlantic University's Ocean Explorer (OEX) AUV as a platform for oceanographic measurements were described. The 12-h shallow-water AUV survey described here is an extension of these earlier efforts. The shallow-water region surveyed lies between two long-shore coral reefs and is subject to very complex flows involving interaction between horizontal shear layers along the edge of the Florida current, the winds and the coastal morphology. Detailed discussion of the 29-day time series of the OSCR measurements during summer 1999 and ship-based measurements of currents, temperature, and salinity are described in [3] and [4]. The focus of the present paper is on AUV-based measurements, including its comparison with OSCR and other fixed and moored instruments. The OEX and its instrument payload are described in Section II. The experiment, the site of the survey, background conditions, and the observations are described in Section III.

II. Instruments

A. The Ocean Ecplorer (OEX) AUV and Onboard Sensors

The OEX series AUV is described in detail by Smith *et al.* [17]. It is a Gertler series body of 2.13–2.4-m variable length (Fig. 1) and 0.53-m maximum diameter. Its unique feature is a modular bayonet-mount interface between its payload and tail section, allowing easy switching of payloads. The 1.1-m tail section houses navigation, control, and propulsion components whereas a nominal 1-m payload section, which may be extended to 2.4 m, is dedicated to house mission-specific instruments. The OEX, which weighs approximately 180 kg in air, is designed to be nearly neutrally buoyant. Its maximum depth rating is 300 m. Using its on-board rechargeable NiCad batteries, which can provide up to approximately 2 kWh of total energy, the OEX can maintain a cruising speed of 1.5 $m \cdot s^{-1}$ (a speed range of 1–2.5 $m \cdot s^{-1}$) for approximately 10 h continuously between the recharge cycles. Longer missions of the type described here are possible using more batteries.

For navigation and control, the aft section of the OEX houses: 1) a downward-looking 1.2-MHz ADCP (Navigator from RD Instruments), which measures altitude and vehicle velocity with respect to either the water column or ground as well as providing current profiles beneath the vehicle; 2) a Watson Block self-motion package which provides attitude and heading information, including Euler angles, tri-axial body rates, and acceleration; 3) a differential GPS receiver unit; 4) RF ethernet; 5) a Falmouth Scientific Instrument's micro CTD, which provides conductivity, temperature, and depth measurement; and 6) a Motorola 68 060 CPU with a VX Works operating system and 1-Gbyte disk storage capacity for logging significant amount of navigation and environmental data. The presence of the motors and the batteries in the tail section can contaminate compass measurement. Therefore, an auxiliary TCM2 Precision Navigation flux-gate compass mounted in the payload section, instead of the Watson Block, is utilized to provide heading information. The accuracy of vehicle positioning and navigation underwater depends primarily on the TCM2 flux-gate compass and the onboard ADCP that provide heading and speed measurements, respectively. For small AUVs, the interior magnetic signatures are usually significant and such errors must be characterized and compensated for. Typical procedures involve spinning the compass together with the vehicle and building a deviation table for the compass given the existence of a compass rose or another independent heading reference that is more accurate. Prior to the experiment described here, a compass rose was used to build the deviation table, from which a maximum of approximately 3° overall heading error was inferred. That is, over a 1-km-long leg transect, an overall positioning error of approximately less than 50 m is expected. More accurate navigation systems are currently under consideration.

During the mission described here, the AUV carried upward- and downward-looking 1.2-MHz ADCPs, a Falmouth Scientific Instruments (FSI) micro-CTD2 on the bottom, and a custom turbulence package on its nose (Fig. 1). The ADCPs operated in a current profiling mode, measuring the velocity in the water column at 16 bins above it with a vertical resolution of 0.5 m and at 16 bins beneath it with a vertical resolution of 1.5 m. The current measurements were interleaved with bottom tracking measurements, both at a sampling rate of 2 Hz. The turbulence package is an updated version of the one described by Dhanak and Holappa [9]. During the experiment described here, it included two shear probes for measurement of cross components of microstructure velocity and a fast-response FP-07 thermistor.

To allow for GPS fixes, the OEX was programmed to surface periodically during its mission. The AUV location was also continuously tracked acoustically via a USBL transponder from the research vessel, FAU's R/V Stephan. The latter was also used to launch and recover the AUV and to provide supplementary ship-based CTD and ADCP measurements. During the missions, 113 different variables were recorded on the AUV

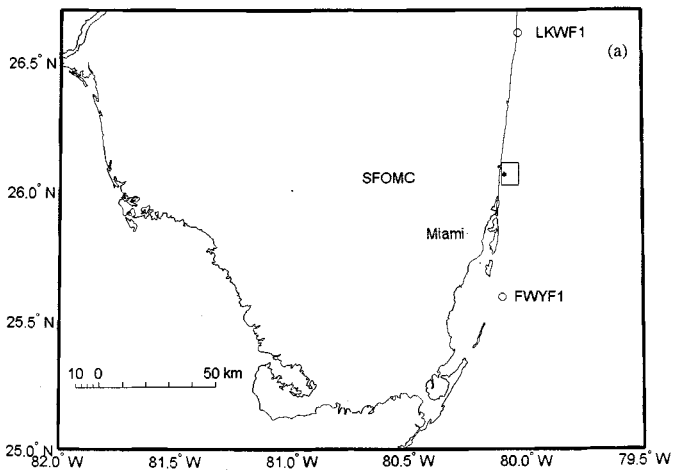

(a)

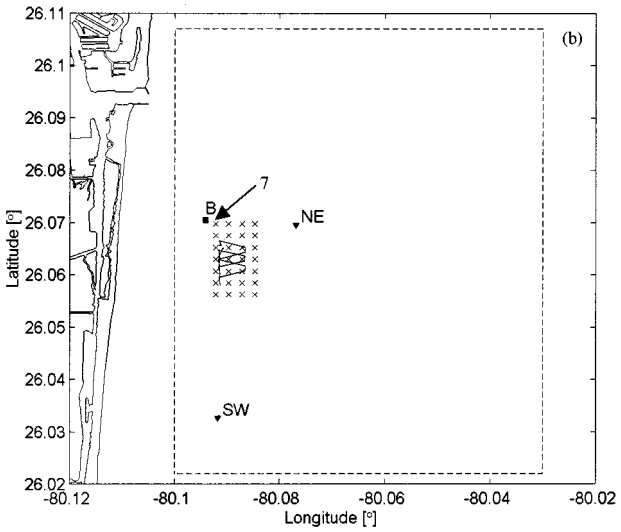

(b)

Fig. 2. (a) Site location off the east coast of Florida. The rectangle marks the OSCR observational field and the shaded area within marks the AUV survey region. (b) Close-up map of the survey region. The dashed rectangle approximately denotes the OSCR coverage region and some of the grid points are shown as "x." The AUV path over the grid points is depicted in the figure.

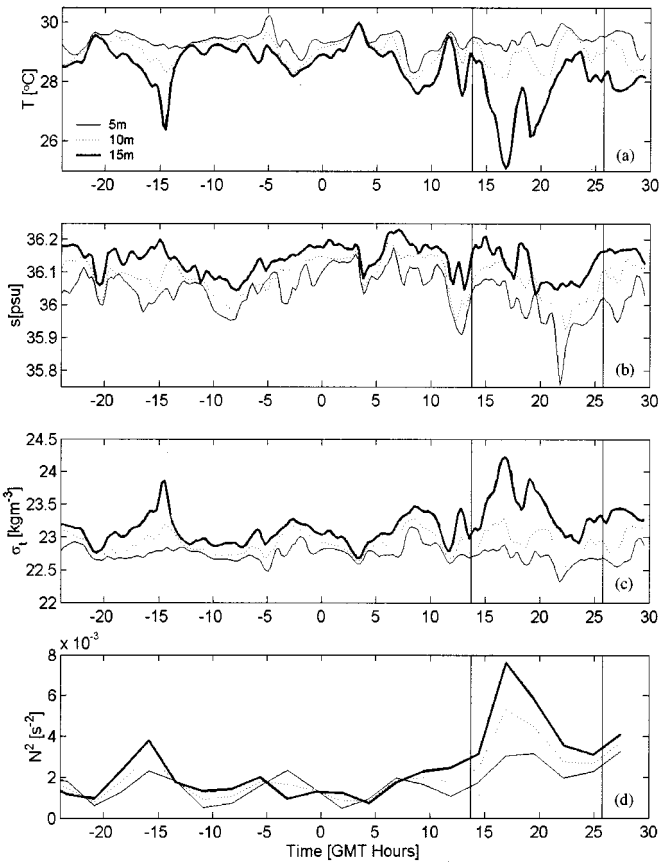

Fig. 3. Time series of: (a) temperature, (b) salinity, and (c) density recorded at the NE USF-NCUa CT chain array buoy at three depths during July 26–28, 1999, and (d) associated variation of the buoyancy frequency (2.5-h average) at the three depths. The time origin marks the start of July 27 and the vertical lines mark the start and end times of the AUV survey.

on-board computer, including instantaneous vehicle position in latitude and longitude, vehicle depth and altitude, current profiles at the vehicle location, and *in situ* conductivity and temperature. The turbulence package separately stored the microstructure data, acquired at 450 Hz.

B. OSCR and Ship-Based Sensor Measurements

The dual-frequency OSCR of the University of Miami, described in detail by Haus *et al.* [1], can use HF (25.4 MHz) and VHF (49.9 MHz) radio frequencies to map surface current patterns over a large area in coastal waters. The shore-based radar system consists of two units (master and slave) deployed several kilometers apart. Each unit acquires independent measurements of current speed along radial beams emanating from its phased-array antennae system. The data are then combined via UHF or telephone communication to produce accurate vector currents (speed and direction), store them to disk, and display them in near real time. The measurements can be made simultaneously at up to 700 grid points either at 1-km (HF mode) or 250-m (VHF mode) nominal resolution and current vector maps developed at intervals of 20 min. In the experiment described here, the OSCR was made to operate in its VHF mode [3], [18]. The maximum range in VHF mode is 11 km where the master and slave stations were located at the U.S. Navy Test Facility (phased array deployed in John U. Lloyd State Park) and Hollywood Beach. This equates to a baseline distance of 6 km, which is optimal for VHF radar mapping of the surface velocity. Over the course of this experiment, a 29 days of continuous time series was acquired where data return approached 97%.

FAU's R/V Stephan was used to carry out periodic casts of a Seabird CTD and to measure local current profiles in the water column using a ship-mounted 600-kHz ADCP. The ship continuously moved around the AUV survey box, over a path of two OSCR cells removed from the AUV operations [4], stopping periodically for CTD casts around the box.

III. Mixed Layer Survey

A. Site and Flow Description

The AUV survey was conducted over a 926 × 556 m box region, near 26° 3′N and 80° 5′W [Fig. 2(a) and (b)], between the second and third of the shallow long shore reefs found on the east coast of south Florida where the water depth varies from

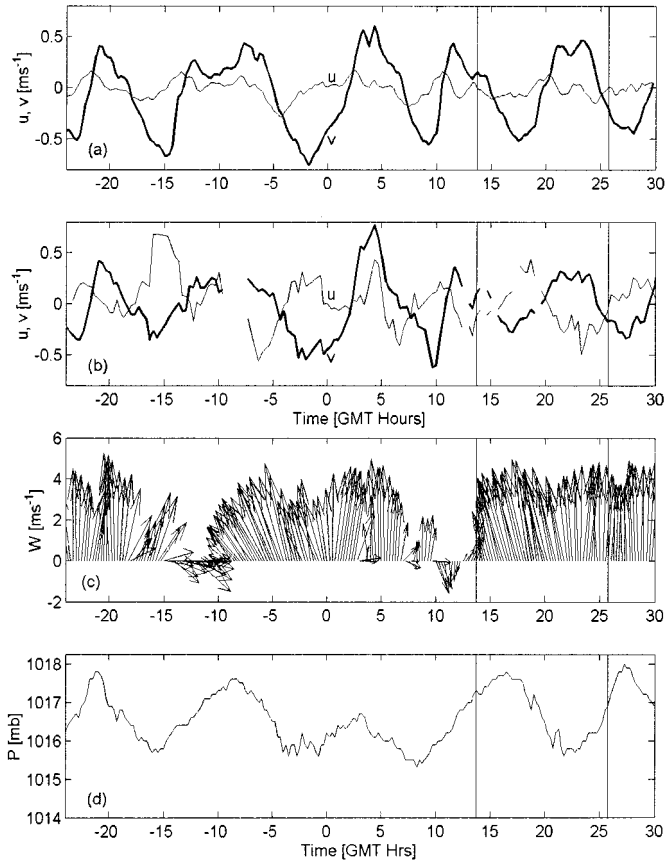

Fig. 4. Time Series of east (u) and north (v) components of: (a) subsurface current at 2.5-m depth recorded at the ADCP B, and (b) of surface current at OSCR grid point 7, (c) winds, and (d) air pressure recorded at the NE buoy. The vertical lines mark the start and end times of the AUV survey.

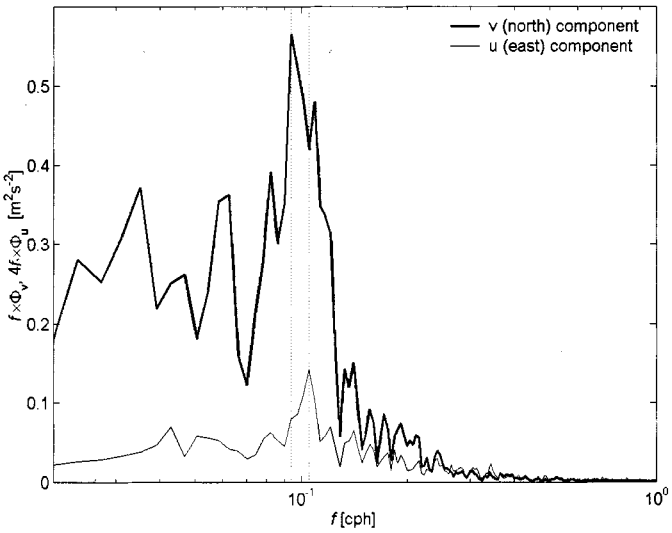

Fig. 5. Power spectra Φ_u and Φ_v for the time series in Fig. 4(a). The dotted vertical lines mark the frequencies 0.093 75 and 0.105 47 cph.

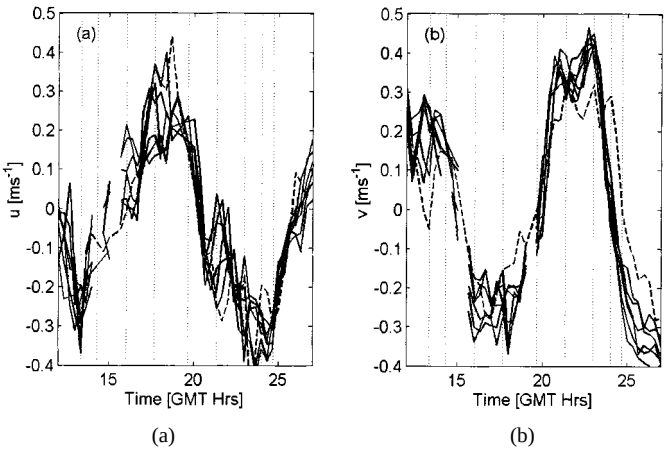

Fig. 6. (a) East–west (cross-shelf) u and (b) north–south (along-shelf) v components of the OSCR time series at six grid points within the AUV survey box and at grid point 7 (dashed line) during the survey. The vertical lines from left to right indicate the times corresponding to the nine synoptic views shown in Fig. 7.

14 to 21 m. The OSCR coverage, in VHF mode, spanned an approximately 6 × 12 km region around the AUV survey box. The Florida current flows east of this region, bearing significant influence on the littoral waters [19]. In particular, the periodic cross-shelf meanders of the Florida current strongly influence the strength of the local currents. Further, eddies shed off the Florida current sometimes slowly propagate along the edge of the current [18]. In addition, the coastal region is influenced by periodic discharge of fresher water from local inlets. During the experiment, the local thermocline was located at around 10–15-m water depth. The characteristics of the mixed layer above the thermocline were studied over a 12-h period.

B. Local Fixed and Moored Instruments and Background Conditions

The surveyed region off Ft. Lauderdale lies within the South Florida Ocean Measurement Center's in-water coastal observatory. During the period of the survey, the following instruments, deployed by the University of South Florida and Nova Southeastern University [20], were operational:

1) A bottom-mounted 300 kHz ADCP, denoted B in Fig. 2(b) and below and located at 26° 4.23′N and 80° 5.65′W in 11-m water depth, recording currents in 0.5-m bins at 15-min intervals. A wave gage was also operational at this site during the survey.
2) A 600-kHz ADCP and a Seabird microcat CT chain array moored from a buoy, denoted SW, in Fig. 2(b) and located at 26° 1.96′N and 80° 5.51′W in 20-m water depth. The ADCP recorded currents in 0.5-m bins and the CT chain array recorded temperature and conductivity at 5, 10, and 15-m water depths, both at 15-min intervals.
3) A 600-kHz ADCP, a Seabird microcat CT chain array moored from a buoy, denoted NE, in Fig. 2(b) and located at 26° 4.17′N and 80° 4.61′W in 50-m water depth. The ADCP recorded currents in 0.5-m bins and the CT chain array recorded temperature and conductivity at 5, 10, and 15-m water depths, both at 15-min intervals.
4) A weather station, recoding wind velocity and air pressure, at 15-min intervals, 2 m above the water surface at the NE buoy. Supplementary atmospheric measurements are made at the NOAA buoys LKWF1 and FWYF1, located north and south of the region [Fig. 1(a)].

The time series of temperature, salinity and density from the NE buoy for July 26–28, 1999 are shown in Fig. 3 for

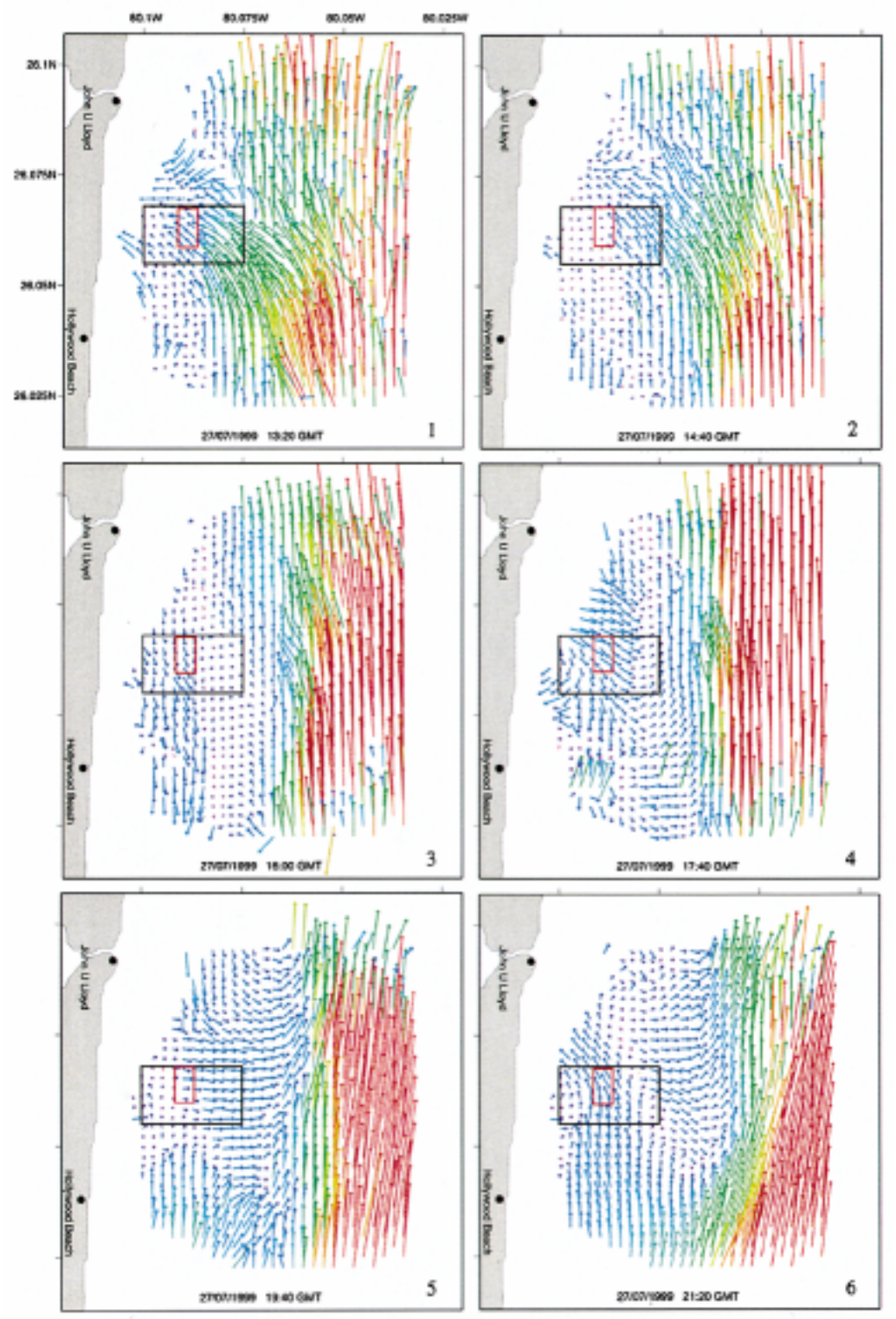

Fig. 7 Nine representative synoptic views of the surface current field over the 12-h period as measured by the OSCR. The velocity vectors are color coded for magnitude. The black box marks the region surveyed by a surface ship and the red box marks the region surveyed by the AUV.

three different depths. The variability of the depth of the thermocline is evident from the figures. It varies from 10 m to beyond 15 m, the mean temperature gradient over the period of the AUV survey being approximately -0.1 °C·m^{-1} in the 5–10 m-depth range, and -0.2 °C·m^{-1} in the 10–15 m-depth range. The time series shown are consistent with corresponding series recorded at the SW buoy, including in the significant dip in salinity seen around 22 h in the 15-m record. The stratification may be characterized by the 2.5-h time-averaged square buoyancy frequency N^2 [Fig. 3(d)], which has mean values of 0.0017, 0.0012, and 0.0024 s^{-2} at depths 5, 10, and 15 m, respectively. Maximum values occurred at around 1650 GMT. The variation in N^2 at the SW buoy is very similar to that at the NE buoy.

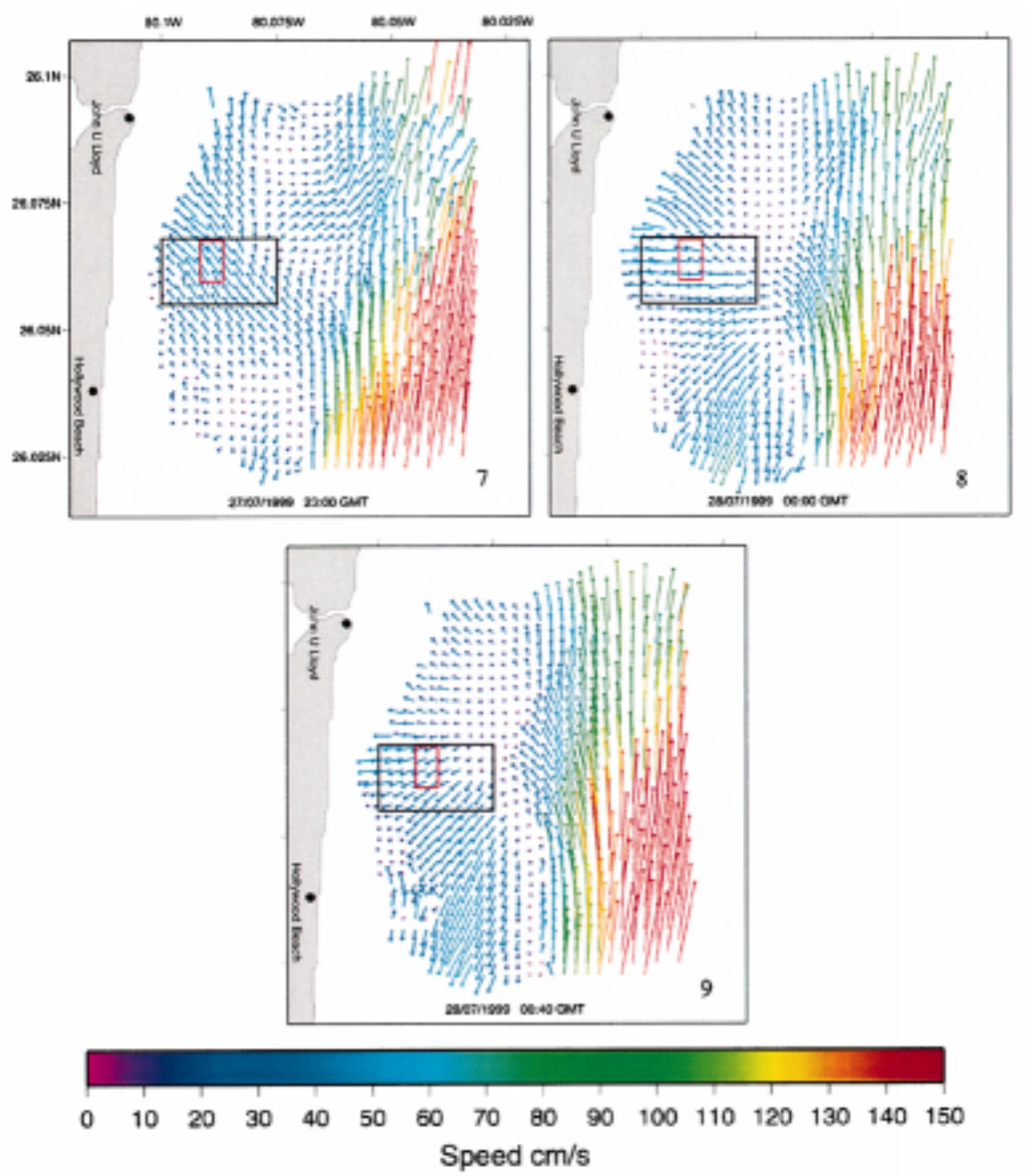

Fig. 7. *(Continued.)* Nine representative synoptic views of the surface current field over the 12-h period as measured by the OSCR. The velocity vectors are color coded for magnitude. The black box marks the region surveyed by a surface ship and the red box marks the region surveyed by the AUV.

The associated time series of the current at 2.5-m depth, recorded at ADCP B, the corresponding surface current at the OSCR grid point closest to B [see Fig. 2(b)], referred to below as grid point 7, the prevailing winds at the NE buoy, and the air pressure are shown in Fig. 4. Both the subsurface [Fig. 4(a)] and surface [Fig. 4(b)] time series clearly show substantial oscillations in both the east–west (cross-shelf) u and north–south (along-shelf) v components of velocity. An analysis of the full (46-day) times series of the fixed ADCP data reveal that the main contribution to the velocity, at least during July 26–28, came from constituents in the frequency range (0.09, 0.11) cph, corresponding to a nominal 10-h oscillation. The spectra of the series (Fig. 5) for u and v have peaks at 0.105 47 and 0.093 75 cph (corresponding to periods of 9.4814 and 10.6667 hs), respectively. From an analysis of the full (29-day) OSCR time series, Peters *et al.* [4] found that, in the case of the surface current, the spectra of both the u and v components exhibit a peak at 0.093 75 cph. In both the ADCP and the OSCR time series, the contributions to u and v due to the S2 tidal constituent do not exceed 0.05 $m \cdot s^{-1}$ and 0.01 $m \cdot s^{-1}$, respectively. Peters *et al.* found that the 10-h oscillatory signal propagated northwards, along the shore, at a phase speed of approximately 0.85 ms^{-1}, and reported that the signals were associated with vorticity or shear waves skin to those observed in nearshore flows (see [21], for example). Away from the shore, Peters *et al.* also observed a presence of a 27-h inertial constituent in the surface currents. They showed that both the 10 and 27-h signals were dominantly barotropic.

The wind and air pressure records at the NE buoy are in general consistent with the corresponding records (not shown) at two CMAN stations, located around 60 km north and south of the region [Fig. 2(a)] and indicate fairly calm atmospheric conditions. Apart from smaller scale variations, we expect this record to be representative of the local winds over the survey

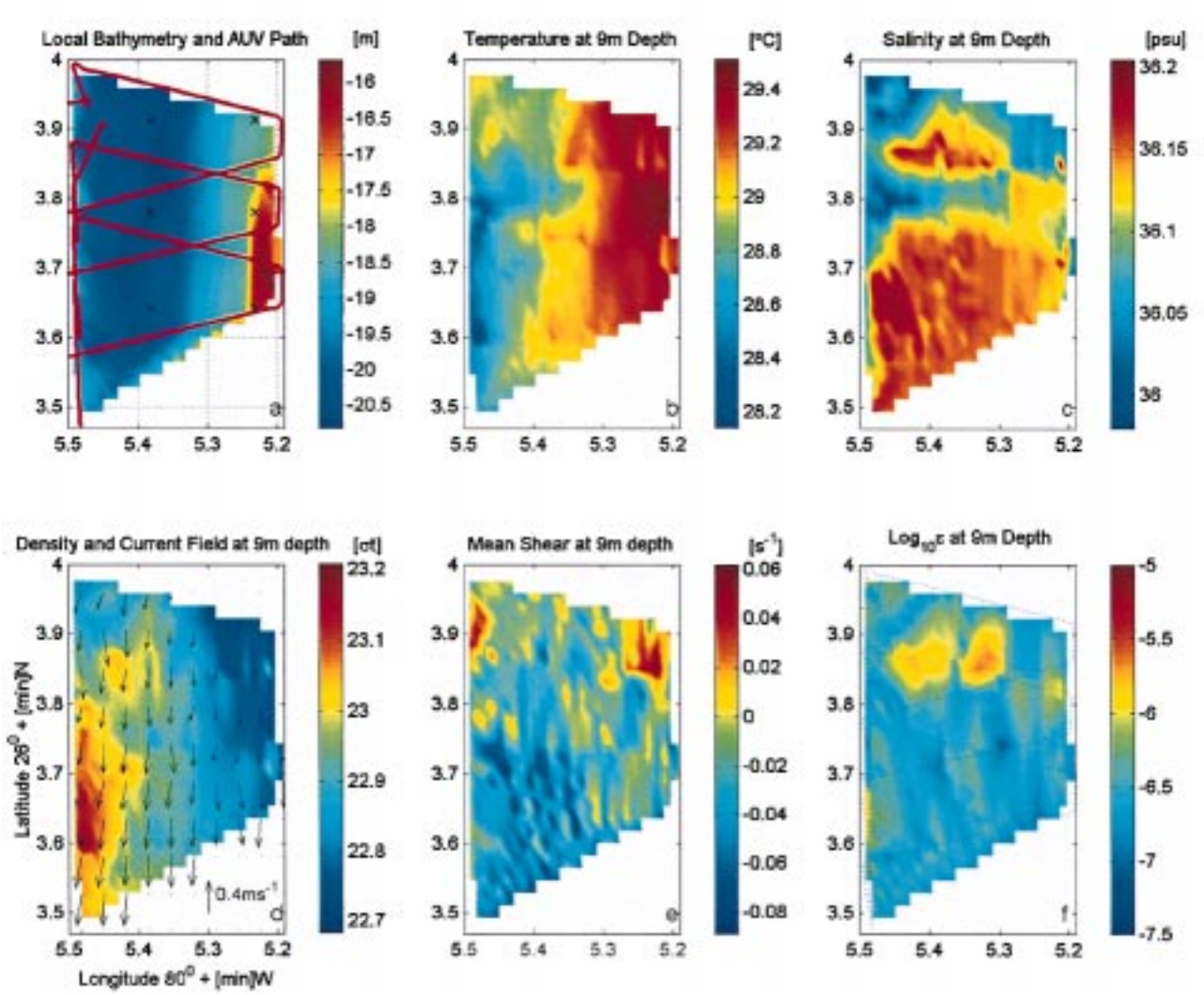

Fig. 8. (a)–(f) Observations from the second segment of the continuous 12-hour AUV survey off the coast of south Florida on 7/27/99. The survey segment shown was carried out during 1524–1646 GMT, giving a nominal mid-range time of 1605 GMT.

box. The winds [Fig. 4(c)] were from the southeast and the speed picked up from 1.5 $m \cdot s^{-1}$ at the start of the AUV survey to a maximum of 5.2 $m \cdot s^{-1}$ at around 1515 GMT, with a mean speed of 4.2 $m \cdot s^{-1}$ over the duration of the 12-h survey. During the survey, the air pressure variation [Fig. 4(d)] did not exceed 2 mbar and 4–5-s-period waves of height not exceeding 0.2 m were recorded at site B.

C. Measurement Survey of July 27, 1999

The 12-hr survey involving AUV-based observations, described here, commenced at 1344 GMT on July 27 and was completed at 0143 GMT on July 28, under monitored background conditions as described above. A general description of all the surveys during July 1999, including a description of the current profile and CTD observations from a surface ship, which moved around the survey box, is given by Shay *et al.* [18]. On July 27, unlike on the other July 1999 surveys, the AUV included sensors for measuring small-scale subsurface turbulence.

1) OSCR Observations: The 29-day OSCR observations over the coverage region identified in Fig. 2(b) during July 1999 are described in detail by Shay *et al.* [3] and by Peters *et al.* [4]. Between them, these papers include a comparison of the OSCR observations with the ship-based and NE moored ADCP observations and an analysis of the OSCR field and the ship-based observations. In this section, we briefly describe the OSCR observations on July 27, particularly over the AUV survey box, relating these to the subsurface AUV-based observations.

The OSCR time series at the six grid points, which were located over the AUV coverage area, and at grid point 7 [see Fig. 2(b)], for the period of the AUV survey are shown in Fig. 6(a) and (b). As is apparent, the 10-h oscillation in both u and v was dominant at each of these grid points. Representative synoptic maps of the surface current field over the 12-h survey are shown in Fig. 7 . The black box in each map nominally marks the region covered by the surface ship and the red box (926 × 556 m) marks the region covered by the AUV [see Fig. 2(b)]. The times of the selected maps approximately correspond to different phases of the current cycle apparent in Fig. 6. The times are sequentially indicated in the latter by dotted lines. As described above and as is apparent from the

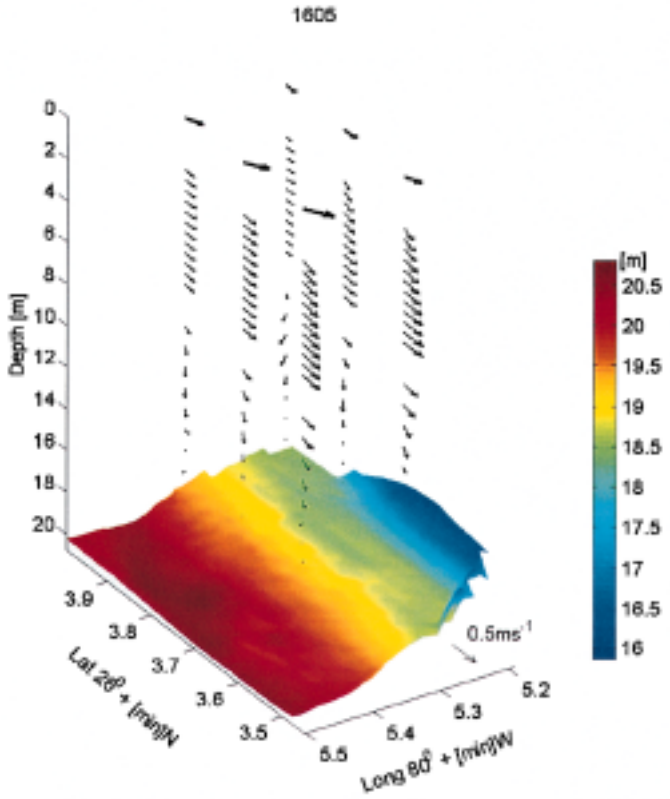

Fig. 9. Current profile of the low-pass filtered (at 15 min) current-field at the six OSCR grid points as determined from the AUV survey during the second segment of the survey. The surface current vectors recorded by OSCR (thicker arrows) are overlaid. The colors indicate the local water depth.

time series in Fig. 6, the surface currents in this shallow-water column were significantly dominated by the 10-h oscillation.

In each map, it helps to discern between the faster moving waters of the Florida current (FC) in the east, with speeds of up to 1.5 $m \cdot s^{-1}$, and the coastal waters, akin to a jet in ambient fluid. A dynamic buffer region, characterized by the presence of horizontal shear layers, marks the edge of the FC. The vector maps in Fig. 7 suggest that the flow was complicated, not only in this buffer region, but also in the entire littoral zone. The wave-like distortions of the buffer region are apparent from the maps in Fig. 7. From an animation of a long series of these maps and from quantitative analysis, Peters *et al.* [4] found that the distortion of the shear layer propagated northwards at speeds of 0.85 $m \cdot s^{-1}$. Such shear waves are associated with a dynamic instability of the horizontal shear layers and appear to be similar to those observed in nearshore flows [21].

The intrusion of the buffer region from the southeast into the region marked by the black box can be seen in maps 1 and 2. The map sequence shows how during the period of the survey, the surface current in the box clocked around, its direction shifting from northwest (1 and 2), to south and southeast (3 and 4), to east (5), to north (6), to northwest (7), to west (8), and to southwest (9).

No coherent vortices, of the type reported by Shay *et al.* [18] in a previous synoptic observation of the region, were apparent in the surface current data during the 12-h observation. The vortices reported by Shay *et al*. were clearly distinguished by circulatory (anticlockwise) patterns in the surface currents. The lack of such features in the present observation may be due to the greater proximity of the FC to the coast in the present case; the resulting strong, oscillatory accelerating flow may act to suppress such vortices.

2) AUV-Based Observations: In order to survey the area, marked by the red box in Fig. 8, in reasonable time, the AUV traveled repeatedly along a path shown in Fig. 8(a) at a preprogrammed depth of 9 m, surfacing periodically to obtain Global Positioning System (GPS) fixes. The portion of the survey shown took around 1.7 h to complete, at an average speed of 1.25 $m \cdot s^{-1}$. The pattern was repeated seven times in the 12-h survey. The bathymetry shown in Fig. 8(a) was obtained through measurement of vehicle depth using the pressure sensor in the onboard CTD package and the measurement of the vehicle altitude using the downward-looking 1.2-MHz ADCP. The latter measures this as well as the vehicle speed over ground and current profiles in the water column beneath the vehicle. The information from the four beams of the ADCP is processed internally in the unit to provide the velocity and altitude data. The accuracy of these instruments is discussed in [10]. In the chosen mode of ADCP operation, the bathymetry resolution is limited by the accuracy in measurement of the vehicle's altitude, depth, and position over the traversed path and density of the vehicle track line in a given coverage area. Throughout the two missions, the bottom track in the shallow water was maintained. At a given point along the vehicle path, the inferred water depth is estimated to be accurate within 1 m while the geographical location of the point is estimated to be within 50 m, taking into accounting the navigational errors. As shown in Fig. 8(a), the 4 –5-m-high ridge of the coral reef east

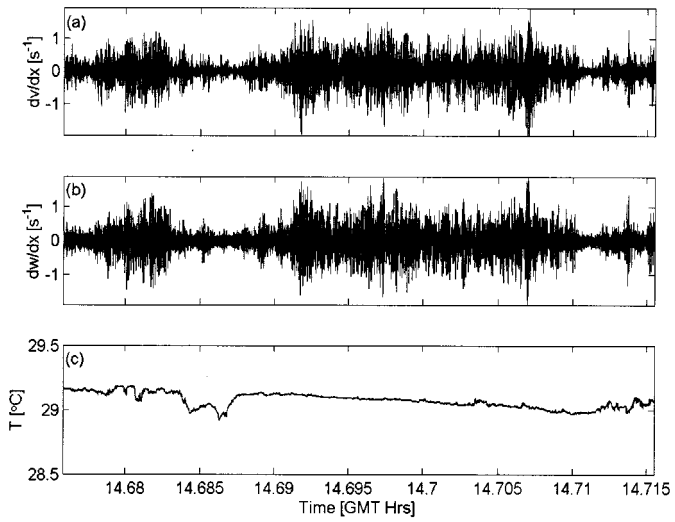

Fig. 10. (a), (b) Two-minute sample microstructure cross-stream shear. (c) Microstructure temperature data.

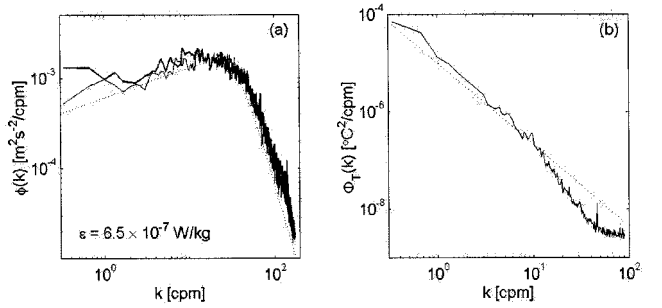

Fig. 11. Spectra of: (a) $\partial v/\partial x$ (thin line) and $\partial w/\partial x$ (thick line) for the time series shown in Fig. 10 (a) and (b), compared with the Nasmyth spectrum (dotted line) and of (b) the temperature time series in Fig. 10(c). The dotted line in (b) indicates $-5/3$ slope.

of the surveyed region is clearly apparent and is consistent with a 1962 U.S. Coast and Geodetic Survey chart.

The recorded water temperature and salinity data from the on-board CTD package for each segment of the survey was used to generate, through interpolation, regional maps of the distribution of temperature, salinity, and water density at 9-m depth for the seven repeated segments of the survey. The maps for the second segment are shown in Fig. 8(b)–(d). It may be noted that these are not synoptic maps; rather, they characterize the spatial distribution of the *in situ* measurements during the mission. Temporal variations on the scale of mission duration or smaller cannot be resolved accurately in such a map. However, temporal variability on a larger scale can be captured from a sequential series of such maps generated from the survey repeated over a significant period. The maps show that, during the period, at 9-m depth, waters in the eastern part of the region are generally warmer and less dense than in the western part of the box. The mean temperature in the box was 29.1 °C, and the difference between the minimum and maximum measured temperature over the second segment was about 1.3 °C. South of the region, the water at the 9-m depth was relatively more saline, the mean value of salinity being 36.04 psu and the difference between the minimum and maximum values being about 0.2 psu.

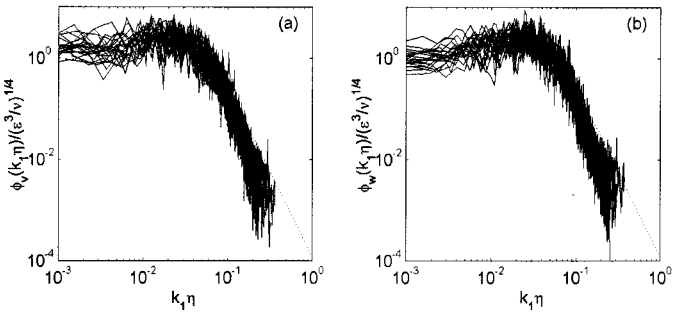

Fig. 12. Normalized shear spectra for: (a) $\partial v/\partial x$ and (b) $\partial w/\partial x$ for the time series in Fig. 10 (a) and (b), compared with the Nasmyth spectrum (dotted line). Twenty-seven spectra, using 5-s samples over the 2-min sample time series, are shown.

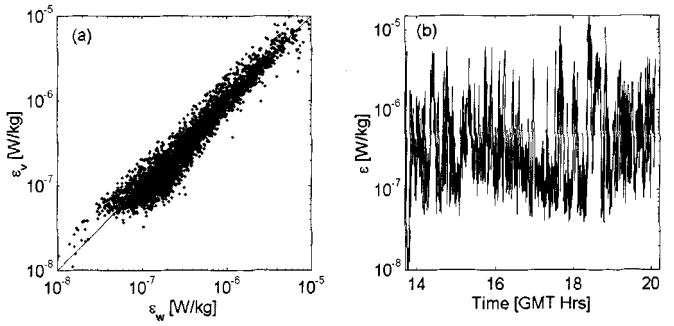

Fig. 13. (a) Dissipation rates ε_v and ε_w as simultaneously determined over 5-s segments from the cross-stream fine-scale shear measurements by the two shear probes. (b) The mean dissipation rate $\varepsilon = (\varepsilon_v + \varepsilon_w)/2$ as a function of time.

The associated mean density was 1022.8 kg·m^{-3} with a variation in the range of about 0.5 kg·m^{-3}.

The two 1.2 –MHz ADCP were programmed to record the velocity profile of the flow above the vehicle at a bin spacing of 0.5 m and beneath the vehicle at a bin spacing of 1 m. The current field at 9-m depth during the second segment, developed from these measurements, is overlaid in Fig. 8(d). The currents at the 9-m vehicle depth were obtained through interpolation from the currents measured by the upward and downward looking ADCPs. The inferred local vertical shear at 9 m and the rate of dissipation of turbulent kinetic energy determined from the *in situ* turbulence measurements were used to develop maps shown in Fig. 8(e) and (f), respectively. The flow in the northwest part of the box is relatively more sheared. Over two distinct patches in the northern part of the surveyed region, the dissipation rates are relatively high, being of $O(10^{-6}$ W kg$^{-1})$ or higher. The corresponding low values of the local mean velocity shear suggest that the small-scale turbulence is not shear related, but may be related to internal wave activity associated with the horizontal variations in density [Fig. 8(d)]. The vehicle path is overlaid on the map in Fig. 8(f) to illustrate the relation between the points where the measurements were made and the interpolated map.

Low-pass filtered (at 15 min) velocity profiles in the water column, determined from the AUV ADCP time series for the second segment of the survey at the six OSCR grid points shown in Fig. 7(a), are shown as three-dimensional (3-D) vector plots in

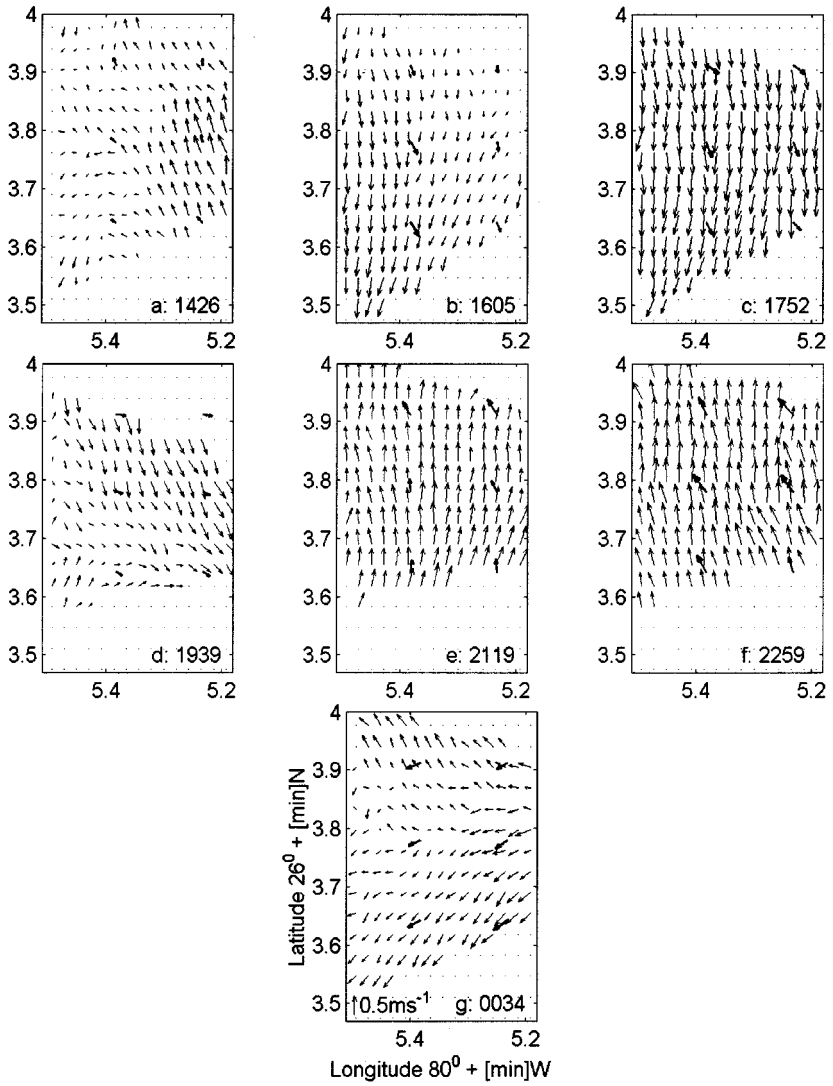

Fig. 14. Maps of the current field at 2.5-m depth as determined from the AUV ADCP measurements and at the surface by OSCR (thicker arrows). The time (GMT) shown in each of the maps (a–g) denote the mid-point of the period of each segment of the survey and approximately correspond to times shown in Fig. 7.

Fig. 9. The figure also shows the corresponding OSCR measurements at the grid points at 1600 GMT. From Fig. 4, a presence of southeasterly winds of around 4 m·s^{-1} is evident during the period. As described above, the thermocline during the survey was below 10 m. The vector plots therefore suggest an almost slab-like flow in the mixed layer above the AUV, compared with a rapid clockwise rotation of the velocity vectors below, the magnitude of the velocity decaying with depth, similar to Ekman spirals induced by wind stress.

Sample time series of the microstructure cross-stream shears

$$\partial v/\partial x = \frac{1}{U_x}\,\partial v/\partial t$$

and

$$\partial w/\partial x = \frac{1}{U_x}\,\partial w/\partial t$$

where v and w are cross-stream components of the turbulent water velocity and U_x is the vehicle speed and microstructure temperature are shown in Fig. 10(a)–(c). The data were recorded at 450 Hz. The turbulence data were processed, as described in [9]. The wavenumber spectra for the sample time series are shown in Fig. 11(a) and (b). Both the shear spectra collapse onto the Nasmyth curve, showing the high quality of the measurements and suggesting local isotropy. The temperature spectra show a $-5/3$ dependence over a significant range, providing a useful check to the shear probe measurements. The measurements can potentially be combined to give an estimate of the distribution of heat flux. The complete data was processed in 5-s segments to determine the distribution of rate of dissipation. Normalized shear spectra over individual time segments, corresponding to the sample time series in Fig. 10(a) and (b), are shown in Fig. 12(a) and (b). The spectra shown were normalized using the Kolmogorov scales for velocity $(\varepsilon/\upsilon)^{1/4}$ and length $(\upsilon^3/\varepsilon)^{1/4}$, where υ is kinematic viscosity and ε the rate of dissipation of the turbulent kinetic energy (TKE). The latter was determined from integration of the spectra over the wavenumber range in the usual way. There is good agreement between the shear spectra from the two independent probes, both of which are in turn in good agreement with the Nasmyth spectrum as shown. The regression between ε_w and ε_v, the

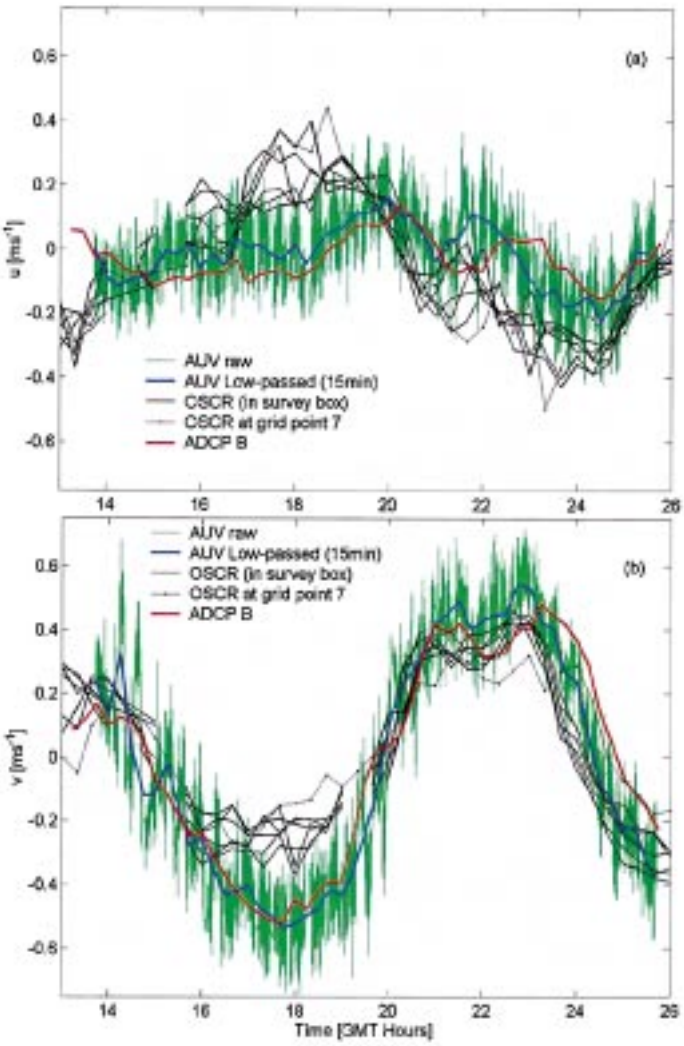

Fig. 15. Time series of: (a) u and (b) v at 2.5-m depth from the AUV and ADCP B records and surface currents from OSCR at the six grid points in the survey box and at grid point 7. The blue line is the AUV data, low-pass filtered at 15 min.

estimates of the dissipation rates evaluated using, respectively, the vertical and horizontal cross-stream spectrum for the various survey segments, is plotted in Fig. 13(a). The regression suggests a good correlation; we take $\varepsilon = (\varepsilon_w + \varepsilon_v)/2$. The variation of ε with time over the first four segments of the survey is shown in Fig. 13(b). The spatial variation of the dissipation during the second segment of the survey is shown in Fig. 8(f) and is described above.

3) Current Comparisons: Comparison of spatial distribution of subsurface currents as determined by the *in situ* measurements from the AUV and the synoptic OSCR maps require caution. First, the AUV maps, such as in Fig. 8, are not synoptic, representing a survey over a period of around 1.7 h. Second, each of the synoptic OSCR maps in Fig. 7, in fact, represents a field developed over 20 min or two legs of the survey pattern shown in Fig. 8(a). Finally, differences between surface and subsurface currents may arise due to such factors as baroclinic flows in strongly stratified regions and wave orbital motion [3]. The map of the current field at 2.5-m depth for

TABLE I
COMPARISON OF AUV-BASED MEASUREMENT OF CURRENT WITH OSCR AND WITH THE BOTTOM-MOUNTED ADCP. γ IS THE COMPLEX CORRELATION COEFFICIENT AND ϕ THE PHASE ANGLE FOR THE RESPECTIVE TIME SERIES, ΔS_{RMS} AND $\Delta\theta_{\mathrm{RMS}}$ ARE THE RMS DIFFERENCES IN SPEED AND DIRECTION, RESPECTIVELY

Subsurface Measurement Depth (m)	Current Comparison Between AUV and OSCR				Current Comparison Between AUV and the Bottom ADCP			
	γ	ϕ (°)	ΔS_{RMS} ms^{-1}	$\Delta\theta_{RMS}$ (°)	γ	ϕ	ΔS_{RMS} ms^{-1}	$\Delta\theta_{RMS}$ (°)
2.5	0.92	-31	0.102	34	0.96	2.33	0.083	18
3.0	0.92	-30	0.102	34	0.95	1.94	0.083	21
3.5	0.91	-30	0.101	34	0.95	2.41	0.087	23
4.0	0.90	-29	0.101	35	0.94	2.39	0.097	25
4.5	0.90	-29	0.102	35	0.93	3.77	0.100	27
5.0	0.89	-28	0.106	35	0.93	2.33	0.101	26
5.5	0.89	-28	0.108	35	0.92	3.32	0.099	28
6.0	0.89	-28	0.108	35	0.91	2.93	0.102	30
6.5	0.89	-27	0.105	35	0.91	1.29	0.103	28
7.0	0.89	-27	0.106	35	0.91	1.27	0.112	29
7.5	0.89	-27	0.103	34	0.91	1.15	0.113	29
8.0	0.90	-27	0.098	34	0.90	0.56	0.116	36
8.5	0.90	-27	0.094	34	0.90	0.03	0.119	64
9.0	0.90	-27	0.094	33				
10.0	0.90	-26	0.101	34				
11.0	0.89	-28	0.101	37				
12.0	0.86	-30	0.113	41				
13.0	0.83	-28	0.130	44				
14.0	0.78	-24	0.158	67				
15.0	0.62	88	0.201	105				

each segment of the survey is shown in Fig. 14. The associated vectors of surface current at the six OSCR grid points in the box are overlaid in each map. In spite of the artifacts mentioned above, there is good qualitative agreement between the OSCR and the AUV measurements in the region, except in maps b–d (see below). The maps illustrate how higher resolution current fields, accompanying a synoptic OSCR observation, may be inferred.

The time series of the AUV and ADCP B observations of the two components of currents at 2.5-m depth are compared with those of the OSCR measurements of the surface current in Fig. 15. The 2.5-m depth is chosen for comparison since it is the closest level to the surface for which subsurface measurements are uncorrupted by surface reflections. The figure depicts times series for: 1) OSCR observations (black line) at grid points in the AUV survey box and at grid point 7 [—•—, see Fig. 2(b)]; 2) AUV-based observations, raw (green curves) and low-pass filtered at 15 min (blue curve); and 3) ADCP B observations (red curve). The spread in the AUV raw data about the dominant frequency motion reflects the local, smaller scale and higher frequency spatial and temporal variability. All three independent observation systems capture the strong 10-h current cycle over the 12-h period. Except between 1600 and 1900 GMT, the agreement between the OSCR and the AUV and the ADCP B observations, at the dominant current frequency, is good. As we note from Fig. 3(d), during 1600–1900 GMT, the stratification in the local water column was relatively strong. Further, developing south-southeasterly winds were present over the region [Fig. 4(c)]. Such effects can introduce discrepancies between the surface and subsurface current field. The developing winds contribute to the surface currents at first, but over time, if they persist, to currents in the entire mixed layer. The possible con-

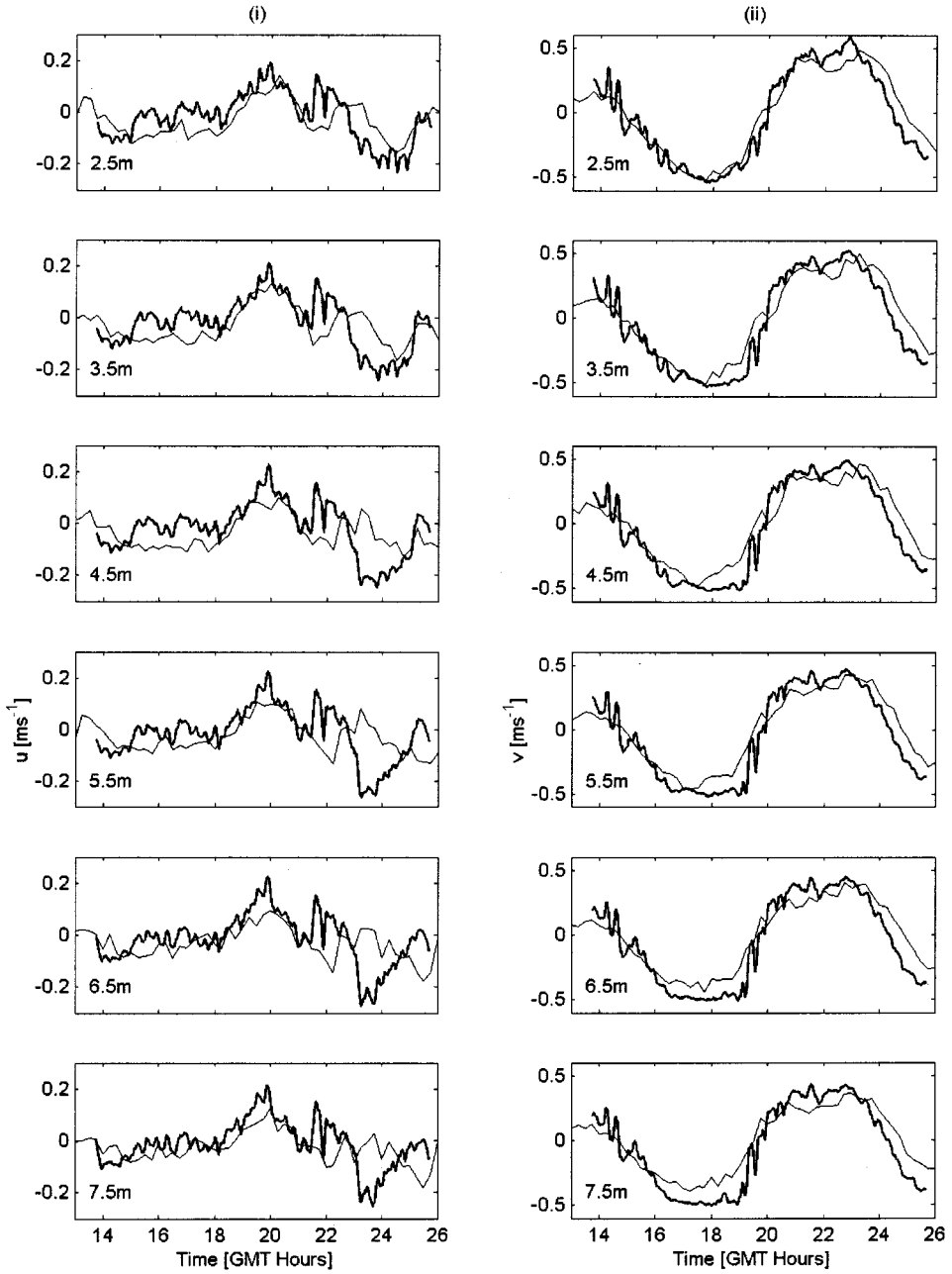

Fig. 16. Comparison between AUV-based (thick line, low passed at 15 minutes) and fixed ADCP (thin line) measurements of: (i) cross-self, u and (ii) along-shelf, v, velocity components at indicated water depths.

tribution of the developing winds to the currents is estimated in the Appendix using available atmospheric data, and it is suggested that the effect may partially account for the discrepancy. The discrepancy may partly be attributed to baroclinicity associated with the presence of a fresher layer above denser layers (see [3]).

The low-passed (at 15 min) AUV time series for u and v components of current at various depths are compared with the corresponding ADCP B series in Fig. 16. The AUV time series for the 8.5- m depth were determined by interpolation. The agreement is generally good except after 2330 GMT, particular at deeper bins. This is believed to be associated with baroclinic effects in view of the particularly dynamic density variations in the region at the time [Fig. 3(b)].

A statistical comparison between the various time series is provided in Table I, which gives values of the complex vector correlation coefficient γ and phase ϕ [21] and rms differences in speed and direction for comparison between OSCR and AUV observations and between ADCP B and AUV observations. To provide a fairer comparison between the OSCR and AUV observations, the latter was averaged over $\pm$2.5-min segments centered on the OSCR sample time and compared with the observation at grid point closest to the AUV over the time segment. Low-passed (at 15 min) AUV series were used for comparison with the ADCP B. The table suggests that the agreement with the ADCP B was generally better than with OSCR, with values of $\square$ in the range 0.9–0.96 for the former, compared with 0.89–0.92 for the latter, for depths less than 9 m. The corresponding ranges

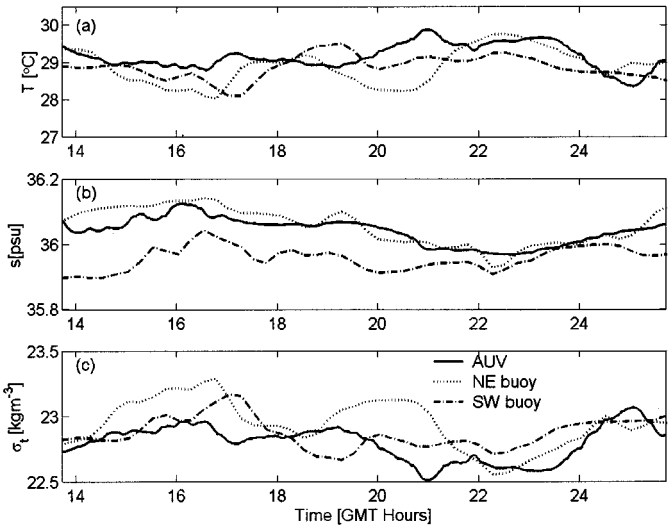

Fig. 17. (a) Temperature, (b) salinity, and (c) density variations during the survey determined from the AUV CT measurements (at 9 m) and the NE and SW USF-Nova CT chain array measurements (at 10 m). AUV conductivity measurements have been adjusted by a constant value of 0.8574 mmho (1.43%) through matching the mean value over the 12-h survey with the mean recorded at the nearby NE CT array.

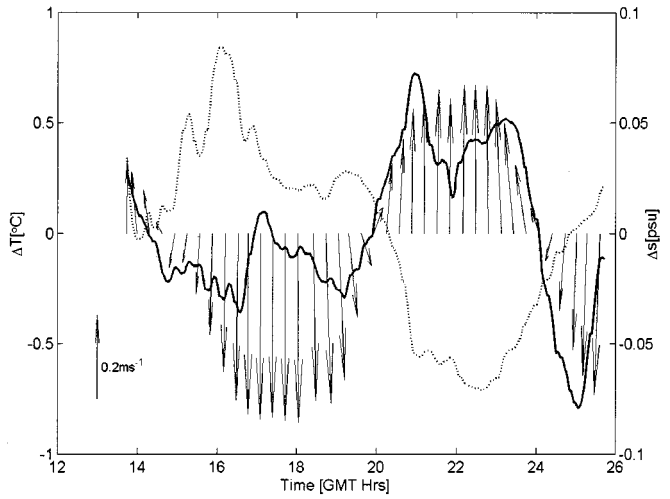

Fig. 18. An overlay of current vector field at 9-m depth, temperature variation ΔT (thick line), and salinity variation Δs, (dotted line) as determined from the AUV measurements. Each time series has been low-pass filtered at 15 min.

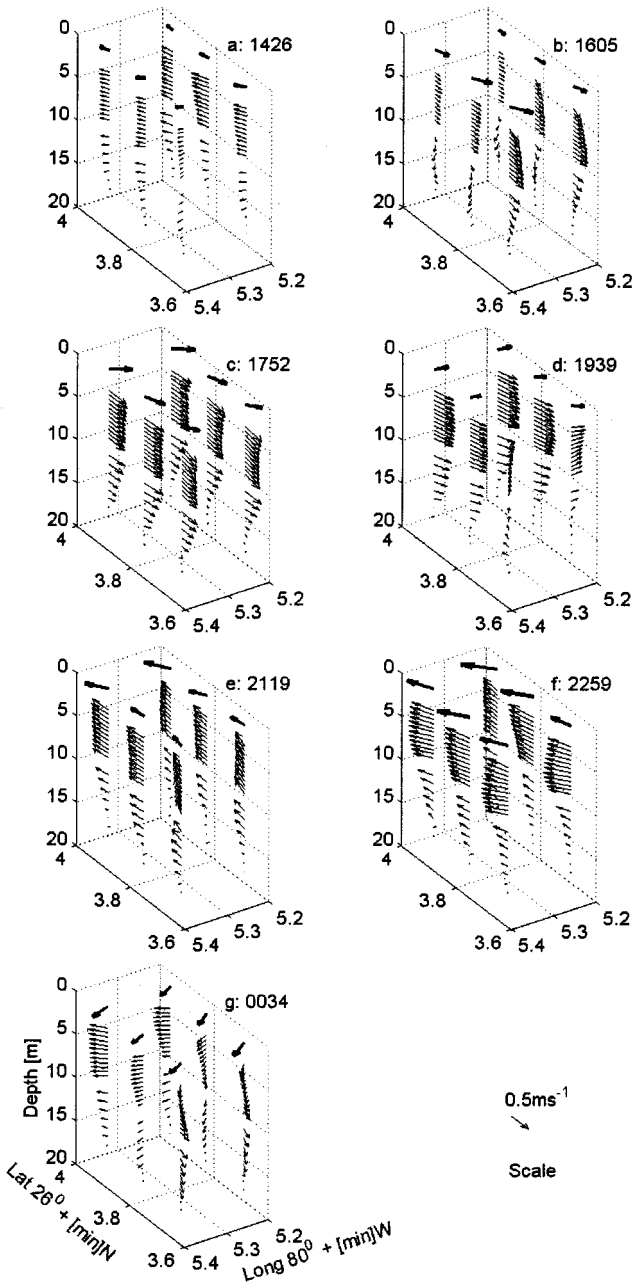

Fig. 19. Current profiles (low-passed at 15 min), overlaid with OSCR surface current records (thick arrows), corresponding to insets in Fig. 14.

for ϕ are 0.03°–3.77° and −27°−−31°, the negative values indicating clockwise rotation of the subsurface field relative to surface currents. The rms differences in speed and direction at 2.5-m depth are 0.083 m·s^{-1} and 18° for the AUV-ADCP B comparison and 0.102 m·s^{-1} and 34° for the AUV-OSCR comparison. The agreement generally gets poorer with depth, as expected.

4) CTD Comparisons: The variation of *in situ* temperature, salinity, and density recorded by the AUV at 9 m depth are shown as time series in Fig. 17 and are compared with corresponding series recorded at the NE and SW buoys [Fig. 2(b)]. There is good agreement between the AUV temperature time series record and the corresponding series recorded at the two buoys. The conductivity recorded by the AUV needed to be adjusted by a constant value of 0.8574 mmho (1.43%) to match the time-averaged mean value with that at the NE buoy (the closer of the two buoys). Such an adjustment represents a cross calibration of field instruments and has been consistently applied to the results presented in the paper. The variation in the resulting AUV time series for salinity closely matches that at the NE buoy. While the temperature and density records at the two buoys match fairly well, the SW location was relatively more saline during the survey, suggesting that density variations were principally governed by temperature variations in the region.

The variations in temperature ΔT and in salinity Δs about the time-averaged mean values are plotted in Fig. 18. The variations appear to be well correlated with the current field at the 9-m depth, which is overlaid on the figure. The figure suggests that relatively cooler, more saline waters were generally advected

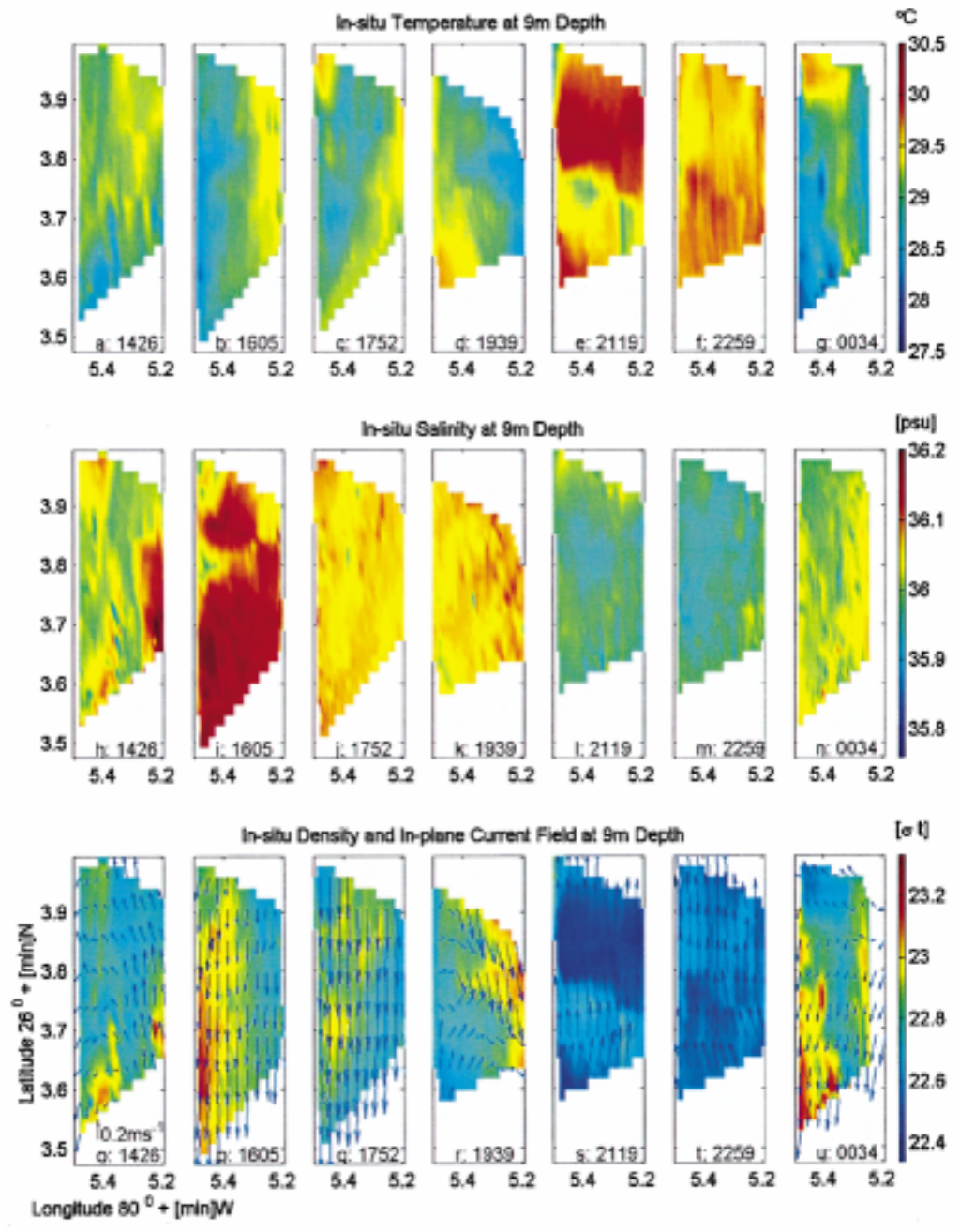

Fig. 20. Maps of the developing temperature (a–g), salinity (h–n), density, and current distributions (o–u) in the survey box at 9-m depth as determined by the AUV observations.

into the survey region from the north during the first half of the current cycle, and were followed by the advection into the AUV survey region of relatively warmer, less saline waters from the south.

5) Evolution of the Mapped Fields: The survey maps shown in Fig. 8 were developed for the other segments of the survey to depict the evolution of the mapped fields. These are shown in Figs. 19–21. Fig. 19 shows the 3-D vector maps of the current field beneath the OSCR grid points during the seven segments of the survey. The vertical variation of the vector maps depict the dynamics of the water column: a boundary layer extending over the entire water column when the current was maximum, at approximately 2300 GMT, say (f), and was dominated by barotropic flow, while featuring rapid turning beneath a slab layer at times of low speeds at approximately 1600, and 2000 GMT, say (b, d), presumably when baroclinic flows dominated.

The evolution of the temperature, salinity, and density maps is shown in Fig. 20. The current fields at the 9-m depth are overlaid in Fig. 20(o)–(u). As described above, temperature variations [Fig. 20(a)–(g)] were generally well correlated with the current, resulting in advection into the region of cooler, more saline waters followed by fresher, warmer waters as the direction of the current shifted. In addition, the waters were generally cooler inshore. However, during segment 4 of the survey, the current was southwards in the east of the region and northwards inshore and resulted in warmer waters inshore and cooler waters offshore.

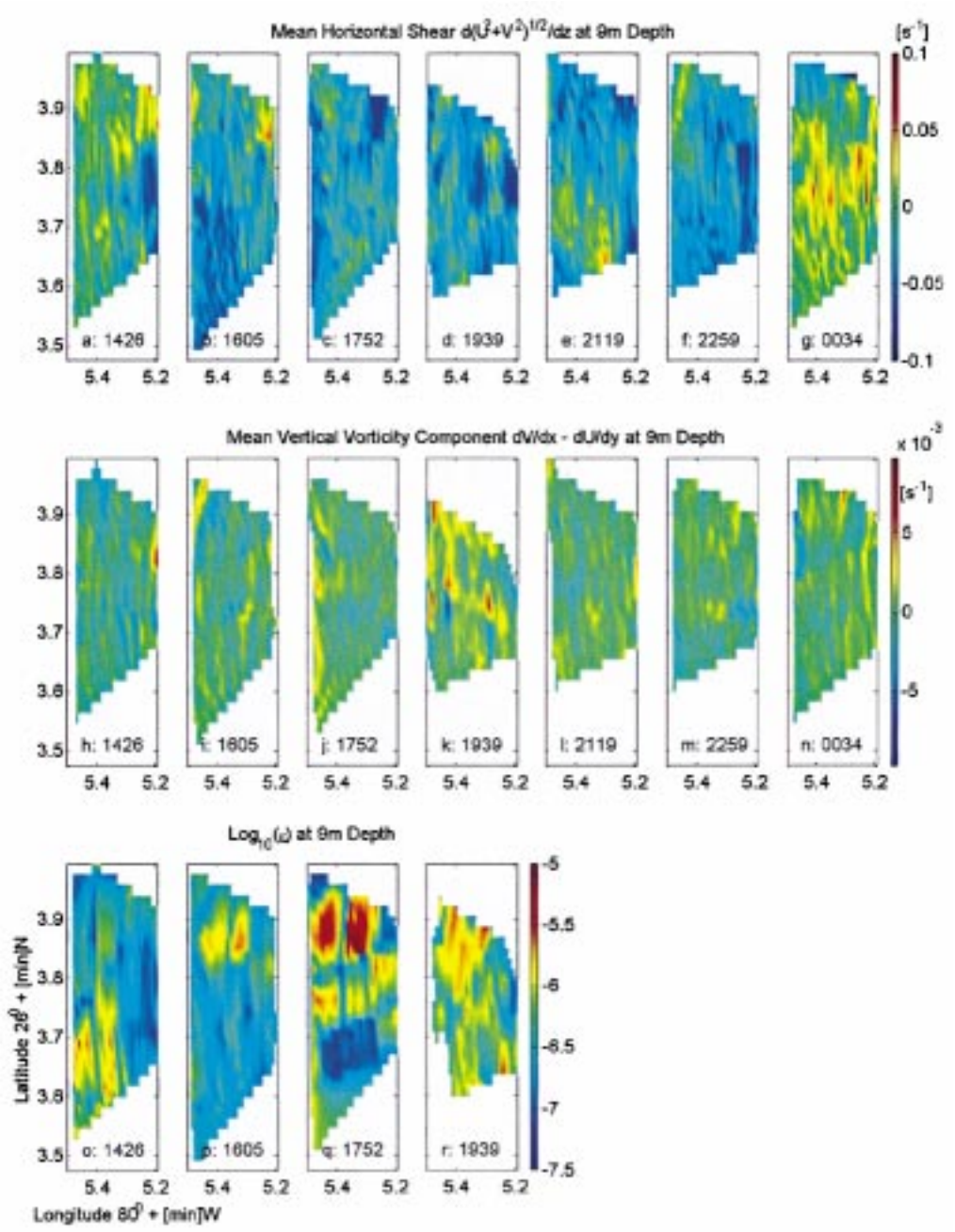

Fig. 21. Maps of the developing mean horizontal shear (a–g), vertical vorticity (h–n), and rate of dissipation (o–r) in the survey box at 9-m depth based on the AUV observations.

Temperatures in the survey box were relatively higher during segments 5 and 6, corresponding to summer evening times with warmer waters advected into the AUV survey box by the north bound current. The waters from the south generally appeared to be warmer, fresher and therefore lighter. The plots depict the near-tidal period variations in the water column during the summer day in the surveyed region along the east coast of South Florida.

The development of the distribution of the mean vertical shear, in-plane mean vorticity and dissipation rates at the 9-m depth are shown in Fig. 21. During the first segment, long patches with relatively high dissipation rates apparently accompanied the low local background currents in the southwest of the survey region. In segments 2 and 3, pairs of patches of relatively high dissipation rates were apparent. As described above, the source of small-scale turbulence in these regions appears to be baroclinic flows associated with horizontal variations in water density. The change of direction of the local current field, apparently involving "collision" of northward and southward traveling water masses, during segment 4 lead to regions of relatively high in-plane vorticity. The dissipation rates were correspondingly higher in these regions. Unfortunately, the turbulence package malfunctioned after continuously collecting data for a 6-h period. The problem appeared to have been associated with overheating inside the package. Since the mission, steps were taken to improve the

heat sink in the package and a subsequent 20-h mission, to be reported elsewhere, was successfully conducted during April 2000.

IV. Summary

AUVs as oceanographic measurement platforms, working in conjunction with traditional methods of data acquisition, can be utilized to resolve the flow field over a range of scales. In a rational approach to oceanography, synoptic maps from satellite or HF radar provide larger scale observation of the surface fields. AUV-based surveys of the type described here and measurements from other moored or bottom-mounted instruments complement the synoptic measurements with observations at smaller scales to develop a better understanding of the processes underlying a particular synoptic observation. Developmental efforts have matured sufficiently to make such an approach feasible.

In the experiment described here, involving an AUV-based survey within the synoptic field of an OSCR, a significant data set over a range of scales, from mesoscale to microstructure, were obtained simultaneously. Details of the dynamic features of the interaction between the Florida current and the coastal zone during a summer day in the mixed layer, off the east coast of Florida, were revealed. The subsurface currents measured by the two ADCPs on the AUV and at site B [Fig. 2(b)] were in general in good qualitative agreement with the surface currents measured by the OSCR, except during a 3-h period when baroclinic and developing wind-driven motion is believed to have led to higher speeds in the subsurface field. Turbulence dissipation rates of $O(10^{-7}$–10^{-5} W/kg) were measured. The relatively high levels of small-scale turbulence observed in patches appear to be baroclinically generated. Maps developed from the survey show how the temperature, salinity, density, currents and dissipation rates in the mixed layer evolved during the observation period.

The work represents a step in the direction of developing an autonomous sampling network, whereby rapid or wide area surveys of the water column can be accomplished to provide higher order temporal or spatial resolution of synoptic fields.

Appendix
Contribution of Winds to Currents

From observation of field data, Ekman reported that (see [16], for example) following a sustained period of prevailing winds

$$V_0 = \alpha W; \qquad D_E = 226.2\alpha W \tag{A1}$$

where W is the wind speed, V_0 is the speed of the induced surface current, D_E is the depth of the Ekman layer, and α is characterized by the latitude of the site. Based on a constant eddy viscosity hypothesis, he found that the direction of the induced surface current was at $\beta = 45°$ (clockwise in the northern hemisphere) to the direction of the wind. From observation, at latitude 26°N, α has a value in the range 0.02–0.05 and typically $\beta < 45°$. The constant in (A1) is obtained using a drag coefficient of $C_D = 1.2 \times 10^{-3}$ and water density of 1023 kgm $^{-3}$.

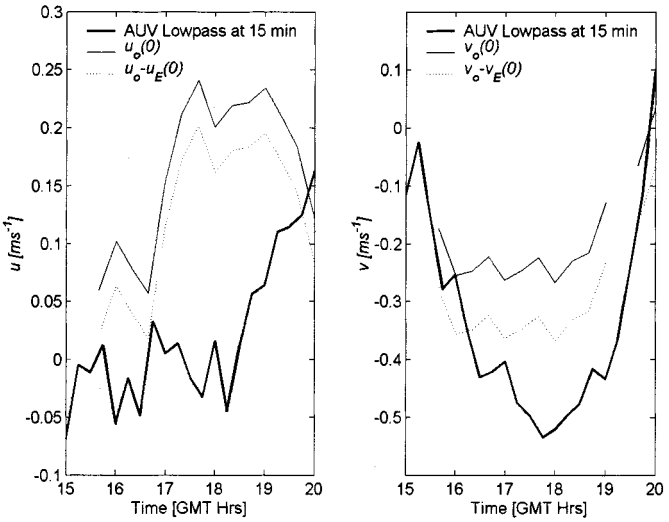

Fig. 22. An estimate of the contribution of the developing wind to the surface current.

The subsurface velocity components in the northern hemisphere are then given by

$$u_E = V_0 \sin(\chi + \beta - \pi z/D_E)\exp(\pi z/D_E);$$
$$v_E = V_0 \cos(\chi + \beta - \pi z/D_E)\exp(\pi z/D_E) \tag{A2}$$

where χ is the direction of the wind and z is measured vertically upwards from the free surface.

During 1600–1900 GMT, the winds were developing and therefore the subsurface contribution may not have been developed. During this period, the mean wind speed was 4.7 m·s^{-1}, measured at 2 m above the surface, which corresponds to 5.44 m·s^{-1} at a nominal height of 10 m. The wind direction was $-24°$. Using these values, and choosing $\beta = 45°$ and $\alpha = 0.02$, we estimate the wind contribution to the surface current to be

$$u_E(0) = 0.10 \ \text{m} \cdot \text{s}^{-1} \quad \text{and} \quad v_E(0) = 0.04 \ \text{m} \cdot \text{s}^{-1}.$$

If the flow were fully developed, we would have at 2.5-m depth

$$u_E(-2.5) = 0.08 \ \text{m} \cdot \text{s}^{-1} \quad \text{and} \quad v_E(-2.5) = 0.004 \ \text{m} \cdot \text{s}^{-1}$$

and the difference would be within the limits of experimental error. However, since the Ekman layer may be developing, we can expect larger differences between the wind-driven surface and subsurface field. We write $u_o = u_R + u_E(0)$ and $v_o = v_R + v_E(0)$, where u_o and v_o are observed components of surface currents and u_R and v_R are associated contributions from sources other than wind. The contribution due to the wind effect to the observed discrepancy can be illustrated as in Fig. 22. Different values of α and β can be considered. On the other hand, the flow development would need to be considered also. The consideration suggests that the developing wind partially accounts for the observed discrepancy.

Acknowledgment

The authors are grateful to M. Chernys, J. Jalbert, and R. Franks of Florida Atlantic University for their part in the ex-

periment and to H. Peters for providing a preprint of Peters *et al.* (2001). The survey was conducted at the South Florida Ocean Measurement Center facility. The OSCR observations, supported by ONR, are due to N. Shay and T. Cook of the University of Miami. The observations from moored and bottom-mounted instruments are due to M. Luther, A. Soloviev, R. Weisberg and associates at the University of South Florida and Nova Southeastern University.

REFERENCES

[1] B. K. Haus, H. C. Graber, L. K. Shay, and J. Martinez, "Ocean surface current observations with HF Doppler radar during the DUCK94 experiment,", RSMAS Tech. Rep. 95-010, p. 104, 1995.

[2] L. K. Shay, S. J. Lentz, H. C. Graber, and B. K. Haus, "Current structure variations detected by high frequency radar and vector measuring current meters," *J. Atmos Oceanogr. Technol.*, vol. 15, pp. 237–256, 1998.

[3] L. K. Shay, T. M. Cook, H. Peters, A. J. Mariano, R. Weisberg, P. E. An, A. Soloviev, and M. Luther, "Very high frequency radar mapping of surface currents," IEEE J. Oceanic Eng., submitted for publication.

[4] H. Peters, L. K. Shay, A. J. Mariano, and T. M. Cook, "Current variability on a narrow shelf with large ambient vorticity," *J. Geophys. Res.*, to be published.

[5] G. Pickard and W. Emery, *Descriptive Physical Oceanography*, 5th ed. New York: Pergamon, 1990.

[6] T. Curtin, J. Bellingham, J. Catipovic, and D. Webb, "Autonomous oceanographic sampling networks," *Oceanography*, vol. 6, no. 3, pp. 86–94, 1993.

[7] J. G. Bellingham and J. S. Willcox, "Optimizing AUV oceanographic surveys," in *Proc. IEEE Symp. Autonomous Underwater Vehicle Technology*, Monterey, CA, 1996, pp. 391–406.

[8] G. Griffiths, N. Millard, S. Mcphail, P. Stevenson, J. Perett, M. Pebody, and A. Webb, "Toward environmental monitoring with the autosub autonomous underwater vehicle," in *Proc. Underwater Technology Conf.*, Tokyo, Japan, 1998, pp. 121–125.

[9] M. R. Dhanak and K. Holappa, "An autonomous ocean turbulence measurement platform," *J. Atmos. Ocean. Technol.*, vol. 16, pp. 1506–1518, 1999.

[10] E. An, M. R. Dhanak, L. K. Shay, S. Smith, and J. Van Leer, "Coastal oceanography using an AUV," *J. Atmos. Ocean. Technol.*, vol. 18, no. 2, pp. 215–234, 2001.

[11] E. R. Levine, D. N. Conners, R. R. Shell, and R. C. Hanson, "Autonomous underwater vehicle-based hydrographic sampling," *J. Atmos. Ocean. Technol.*, vol. 14, no. 6, pp. 1444–1454, 1997.

[12] E. R. Levine and R. G. Lueck, "Estuarine turbulence measurements with an autonomous underwater vehicle," in *Proc. EOS, Trans. AGU*, vol. 76, 1996, OS79.

[13] J. S. Riedel and A. J. Healey, "Estimation of directional wave spectra from an AUV," in *Proc. 11th Int. Symp. UUST'99*, 1999, pp. 140–149.

[14] H. Schmidt, J. G. Bellingham, M. Johnson, D. Herold, D. M. Farmer, and R. Pawlowicz, "Real-time frontal mapping with AUV's in a coastal environment," in *Proc. MTS/IEEE Oceans'96*, Ft. Lauderdale, FL, 1996, pp. 1094–1098.

[15] D. R. Yoerger, A. Bradley, and B. Walden, "Scientific survey with the autonomous benthic explorer," in *Proc. 10th Int. Symp. UUST 97*, Durham, NH, 1997, pp. 41–49.

[16] D. R. Yoerger, A. Bradley, M.-H. Cormier, W. B. F. Ryan, and B. Walden, "High resolution mapping of a fast spreading mid-ocean ridge with the autonomous benthic explorer," in *Proc. 11th Int. Symp. UUST, AUSI*. Durham, NH, 1999, pp. 209–221.

[17] S. M. Smith, K. Heeb, N. Frolund, and T. Pantelakis, "The ocean explorer AUV: A modular platform for coastal oceanography," in *Proc 9th Int. Symp. UUST'95*. Durham, NH, 1995, pp. 67–73.

[18] L. K. Shay, T. M. Cook, B. K. Haus, J. Martinez, H. Peters, A. J. Mariano, P. E. An, S. Smith, A. Soloviev, R. Weisberg, and M. Luther, "VHF radar detects oceanic submesoscale vortex along the Florida coast," *EOS*, vol. 81, no. 19, p. 209, 213, 2000.

[19] T. N. Lee, C. Rooth, E. Williams, M. McGowan, A. F. Szmant, and M. E. Clarke, "Influence of Florida current, gyres, and wind-driven circulation on the transport of larvae and recruitment in the Florida Keys coral reefs," *Cont. Shelf Res.*, vol. 12, pp. 971–1002, 1992.

[20] M. E. Luther, R. H. Weisberg, A. V. Soloviev, and J. P. McCreary, "Environmental array in the South Florida Ocean Measurement Center (SFOMC) and data analysis," in *AGU Winter Meeting*, Dec. 1999, OS32B-07.

[21] A. J. Bowen and R. A. Holman, "Shear instabilities of the mean longshore current. I. theory," *J. Geophys. Res.*, vol. 94, pp. 18,023–18 030, 1989.

[22] P. K Kundu, "Ekman veering observed near the ocean bottom," *J. Phys. Ocean*, vol. 6, pp. 238–242, 1976.

[23] E. R. Levine and R. G. Lueck, "Turbulence measurement from an autonomous underwater vehicle," *J. Atmos. Ocean. Technol.*, vol. 16, pp. 1533–1544, 1999.

[24] S. Pond and G. L. Pickard, *Introductory Dynamical Oceanography*, 2nd ed. London, U.K.: Butterworth Heinemann, 1983.

[25] F. Schott, T. N. Lee, and R. Zantopp, "Variability of the structure and transport of the Florida current in the period range of days to seasonal," *J. Phys. Oceanogr.*, vol. 18, no. 9, pp. 1209–1230, 1988.

Manhar R. Dhanak is Professor and Director of Center for Hydrodynamics and Physical Oceanography at Florida Atlantic University, Boca Raton. His current research interests include oceanic turbulence and dynamics of coherent flow structures. Over the past few years, he has been involved in the development of custom oceanographic sensor systems for implementation on AUVs.

P. Edgar An received the B.S.E.E. degree from the University of Mississippi, University, in 1985, and the M.S.E.E. and Ph.D. degrees from the University of New Hampshire, Durham, in 1988 and 1991, respectively.

After completing his doctoral work, he became a Post-Doctoral Fellow in the Department of Aeronautics and Astronautics at the University of Southampton, Southampton, U.K., working on the European Prometheus project. In 1994, he joined the Department of Ocean Engineering at Florida Atlantic University (FAU), Dania, as a visiting faculty member. He became an Assistant Professor at FAU in 1995, and is currently an Associate Professor. His areas of interest are autonomous underwater vehicles, navigation, control, modeling and simulation, and neurofuzzy systems. His publications include more than 50 journal and conference papers in these research areas.

Dr. An is a recipient of the 1998 FAU Researcher of the Year award for the Assistant Professor level. He is a member of Sigma Xi.

Ken Holappa received the Ph.D. degree in ocean engineering from Florida Atlantic University, Dania, in 1998.

He was an Assistant Professor in the Department of Ocean Engineering at Florida Atlantic University, Boca Raton. He is currently with Ocean Sensor Systems Inc., Coral Springs, FL. His research interests include environmental ocean sensors to monitor and improve the health of the world's oceans.